Electronic Supplementary Information

Anisotropic carrier mobility in buckled two-dimensional GaN

Lijia Tong,[a] Junjie He,[b] Min Yang,[a] Zheng Chen,*[a] Jing Zhang,[a] Yanli Lu[a] and Ziyuan Zhao*[c]

[a]*State Key Laboratory of Solidification Processing, School of Materials Science and Engineering, Northwestern Polytechnical University, Xi'an 710072, PR China. E-mail: chenzh@nwpu.edu.cn*

[b]*Department of Physical and Macromolecular Chemistry, Faculty of Science, Charles University in Prague, 128 43 Prague 2, Czech Republic*

[c]*School of Materials Science and Engineering, Xi'an University of Technology, Xi'an 710048, PR China. E-mail: zhao.ziyuan@outlook.com*
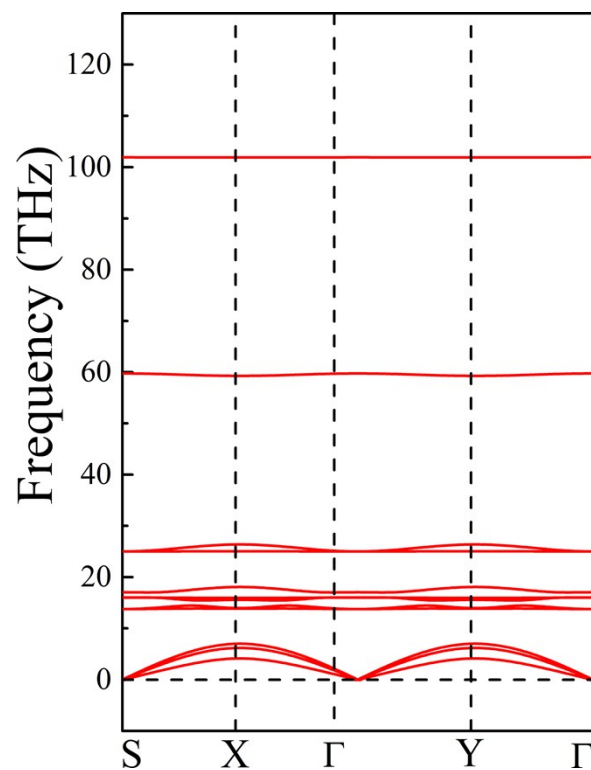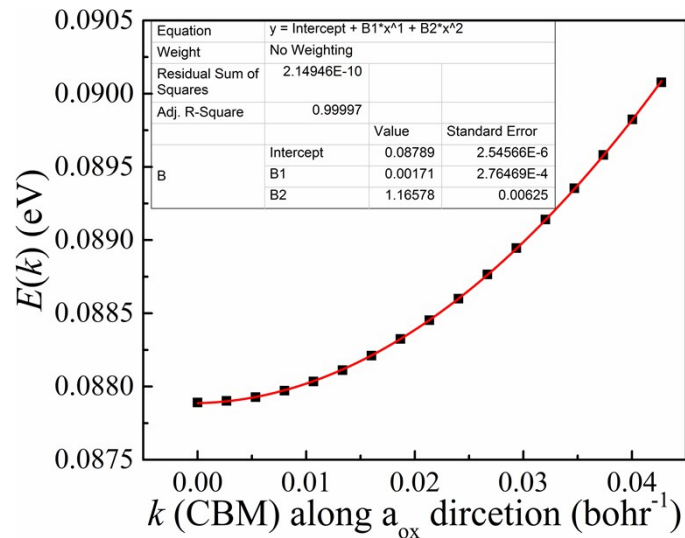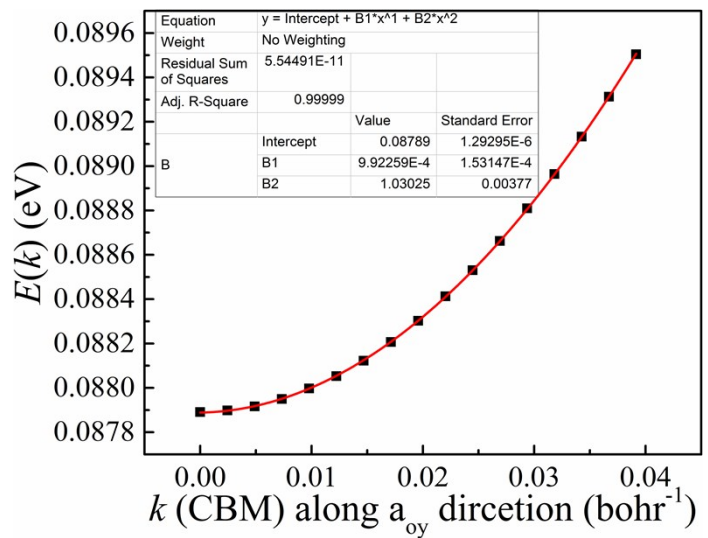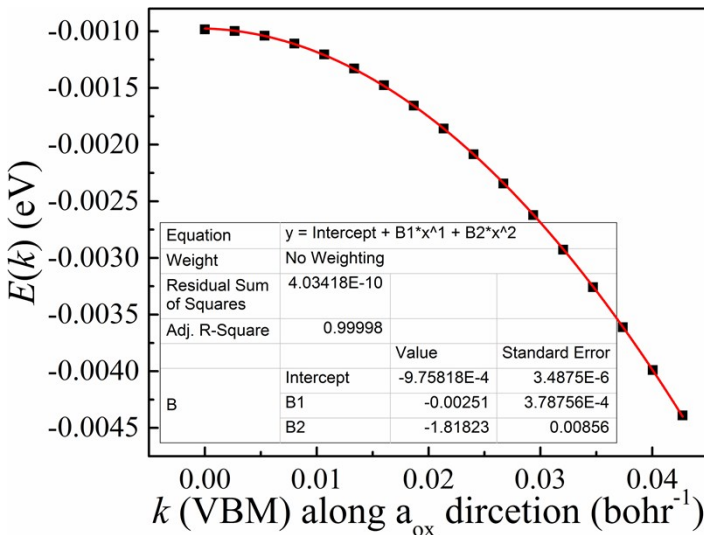
Figure S1. Phonon band structures of HGaNH (orthogonal super cell).

(a)

Equation	y = Intercept + B1*x^1 + B2*x^2	
Weight	No Weighting	
Residual Sum of Squares	2.14946E-10	
Adj. R-Square	0.99997	
	Value	Standard Error
Intercept	0.08789	2.54566E-6
B	B1	0.00171	2.76469E-4
	B2	1.16578	0.00625

(b)

Equation	y = Intercept + B1*x^1 + B2*x^2	
Weight	No Weighting	
Residual Sum of Squares	5.54491E-11	
Adj. R-Square	0.99999	
	Value	Standard Error
Intercept	0.08789	1.29295E-6
B	B1	9.92259E-4	1.53147E-4
	B2	1.03025	0.00377

(c)

Equation	y = Intercept + B1*x^1 + B2*x^2	
Weight	No Weighting	
Residual Sum of Squares	4.03418E-10	
Adj. R-Square	0.99998	
	Value	Standard Error
Intercept	-9.75818E-4	3.4875E-6
B	B1	-0.00251	3.78756E-4
	B2	-1.81823	0.00856

(d)

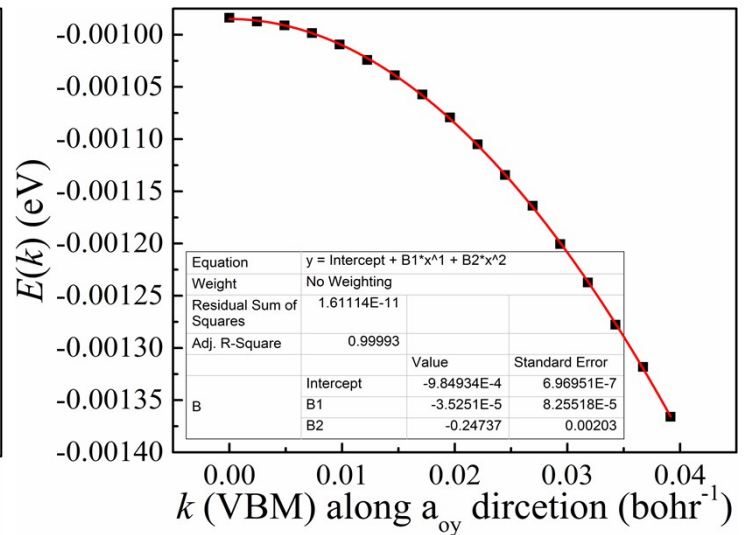| Equation	y = Intercept + B1*x^1 + B2*x^2	
Weight	No Weighting	
Residual Sum of Squares	1.61114E-11	
Adj. R-Square	0.99993	
	Value	Standard Error
Intercept	-9.84934E-4	6.96951E-7
B	B1	-3.5251E-5	8.25518E-5
	B2	-0.24737	0.00203

Figure S2. The fitted curves of $E(k)$-k of FGaNH, where $E(k)$ is the energy of k states around the conduction band minimum (CBM) or valence band maximum (VBM) in the first Brillouin zone, for calculate the corresponding effective masses ($m^* = \hbar^2[\partial^2 E(k)/\partial k^2]^{-1}$) of FGaNH. (a, b) for calculate the electron m^* along a_{ox} and a_{oy} directions. (c, d) for calculate the hole m^* along a_{ox} and a_{oy} directions. Note that the "0.00 point" in the horizontal axis represent CBM or VBM.

According to the definition of effective mass, we first calculate the relationship of $E(k)$-k around CBM\VBM in FGaNH (Fig. S2). Then fitting (quadratic fit) the $E(k)$-k curves (Fig. S2) and m^* is obtained through substituting the quadratic function into the

formula ($m^* = \hbar^2[\partial^2 E(k)/\partial k^2]^{-1}$). Although the "Adj. R-Suqar" of fitted $E(k)$-k curves (Fig. S2) is nearly close to 1 which verifies the validity of the fitting results, the tiny "Standard Error" (0.002~0.009) is also existed. However, according to the report of Wei Ji *et al*. [11], a fitting error of 20% is definitely reasonable considering the accuracy limit of DFT when calculating carrier mobility. Thus, the tiny "Standard Error" ought to have no significant influence on our principal results (the anisotropic μ).
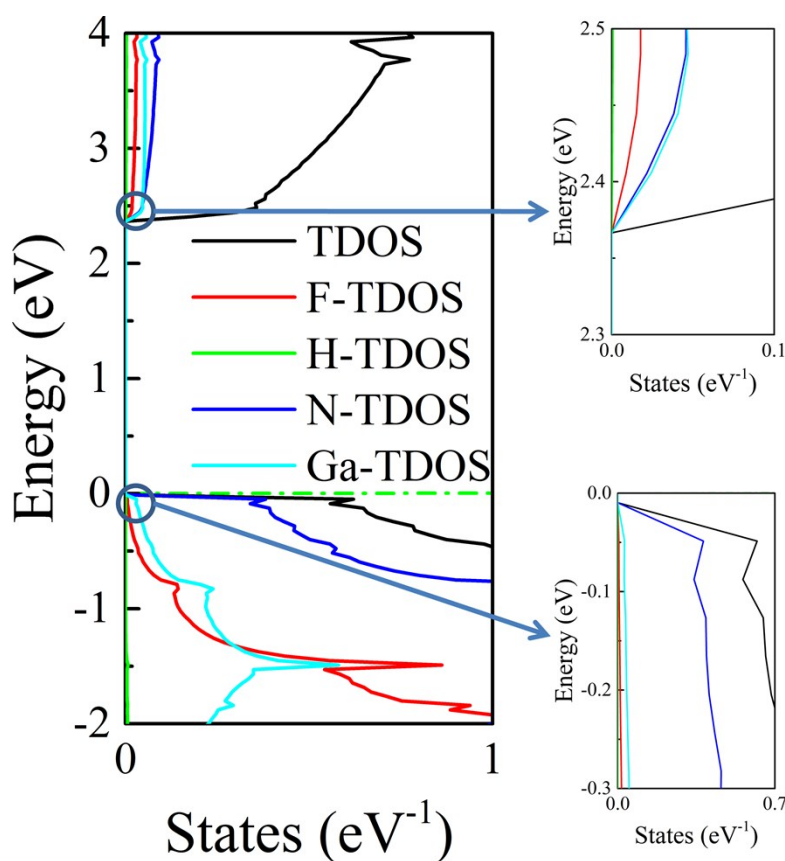
Figure S3. The density of states (DOS) of FGaNH. The right panel shows the enlarged detail around CBM or VBM.
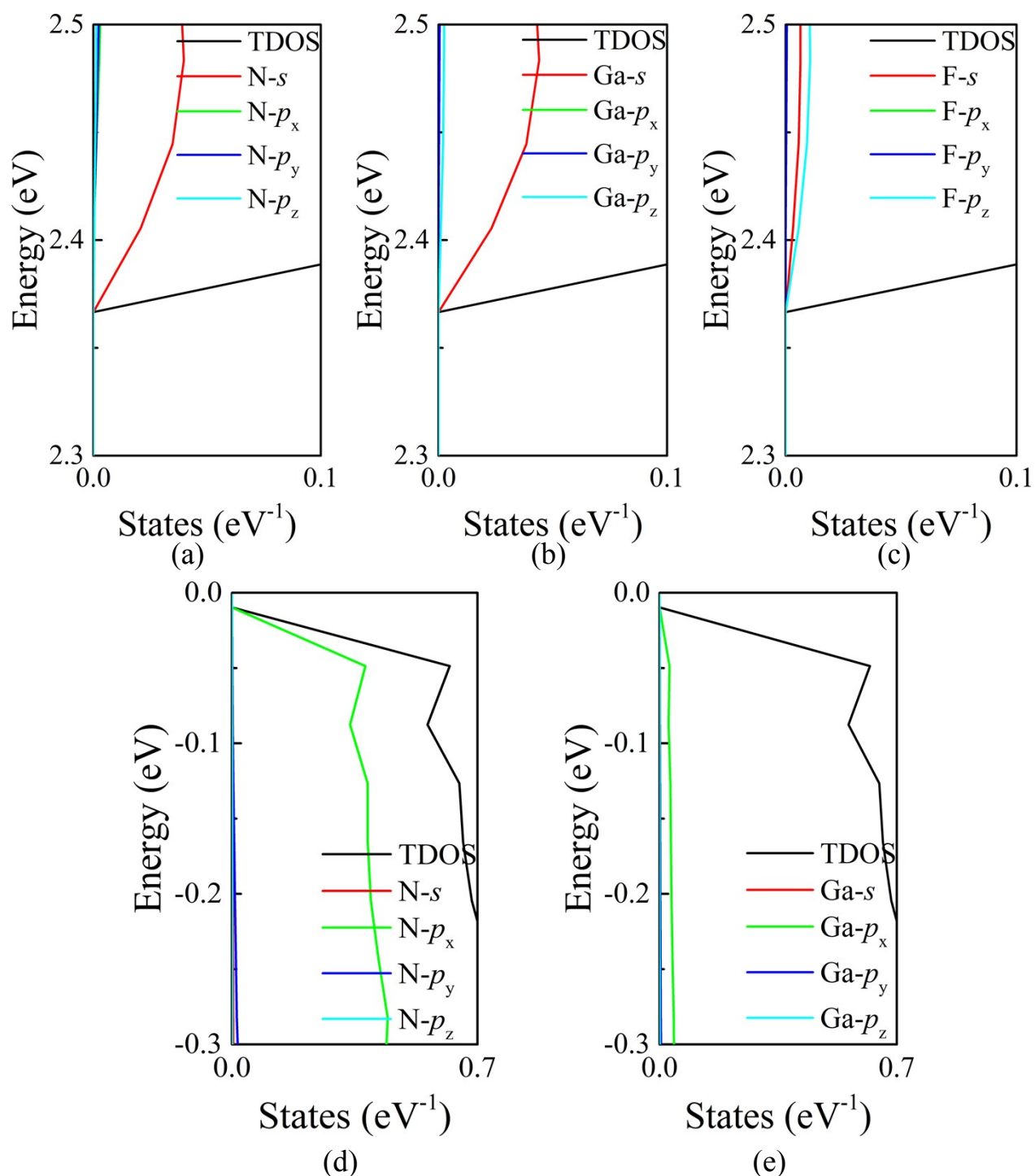
Figure S4. The partial density of states (PDOS) of in-plane N atoms and Ga atoms which constitute the major part of CBM (a and b) and VBM (c and d) in FGaNH.

In order to clarify which atoms contribute to the CBM or VBM in FGaNH, the TDOS of each atoms is shown in Fig. S3. Fig. S3 unambiguously illustrates that the CBM of HGaNH mainly stems from the out-plane F atoms (minor) and in-plan N and Ga atoms

(major), while the VBM of FGaNH only origins from the in-plane N atoms (major) and Ga atoms (minor). Furthermore, to clarify which orbitals of the atoms associated with CBM\VBM of FGaNH, the PDOS of the corresponding atoms are shown in Fig. S4. Fig. S4 (a-c) show that the CBM of FGaNH mainly stems from in-plane orbitals (N-s and Ga-s) and out-plane orbitals (F-s+p_z), while (d) and (e) reveal that the VBM of FGaNH mainly stems from perpendicular (relative to the Ga-N plane) N-p_x orbitals (major) and Ga-p_x orbitals (minor).
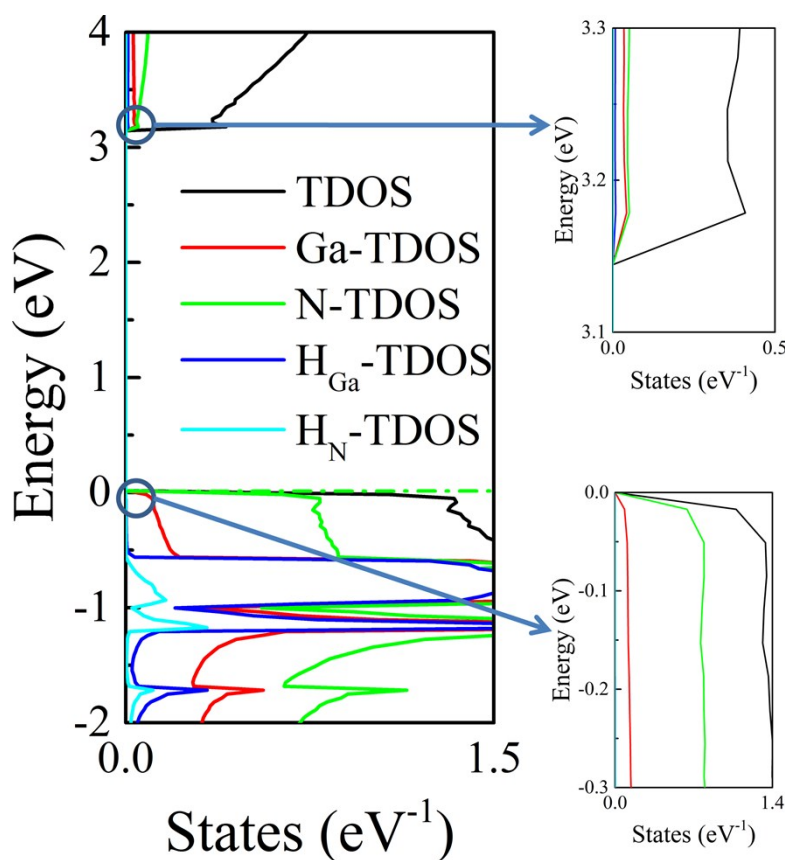

Figure S5. The density of states (DOS) of HGaNH. The right panel shows the enlarged detail around CBM or VBM.

Similarly, the TDOS and PDOS of each atoms associated with the CBM and VBM of HGaNH are shown in Fig. S5 and S6. As seen in Fig. S5 and S6, the CBM of HGaNH mainly stems from in-plane N and Ga atoms (s and p_z orbitals) and out-plane H_{Ga}-s

orbitals, while the VBM of HGaNH mainly stems from perpendicular (relative to the Ga-N plane) N-p_xp_y orbitals (major) and Ga-p_xp_y orbitals (minor).
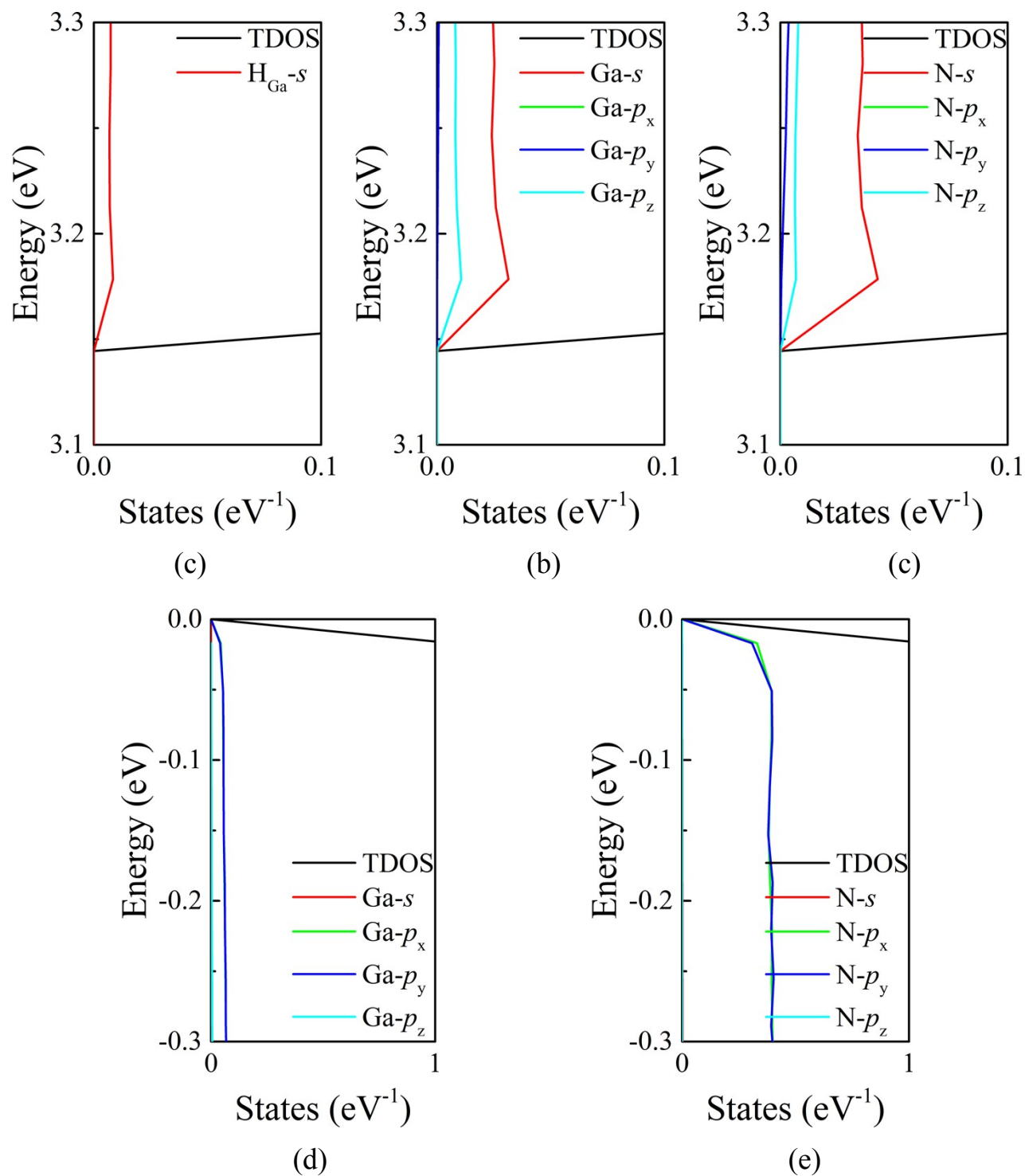

(c)

(b)

(c)

(d)

(e)

Figure S6. The partial density of states (PDOS) of all the atoms which constitute the major part of CBM (a-c) and VBM (d and e) in HGaNH.
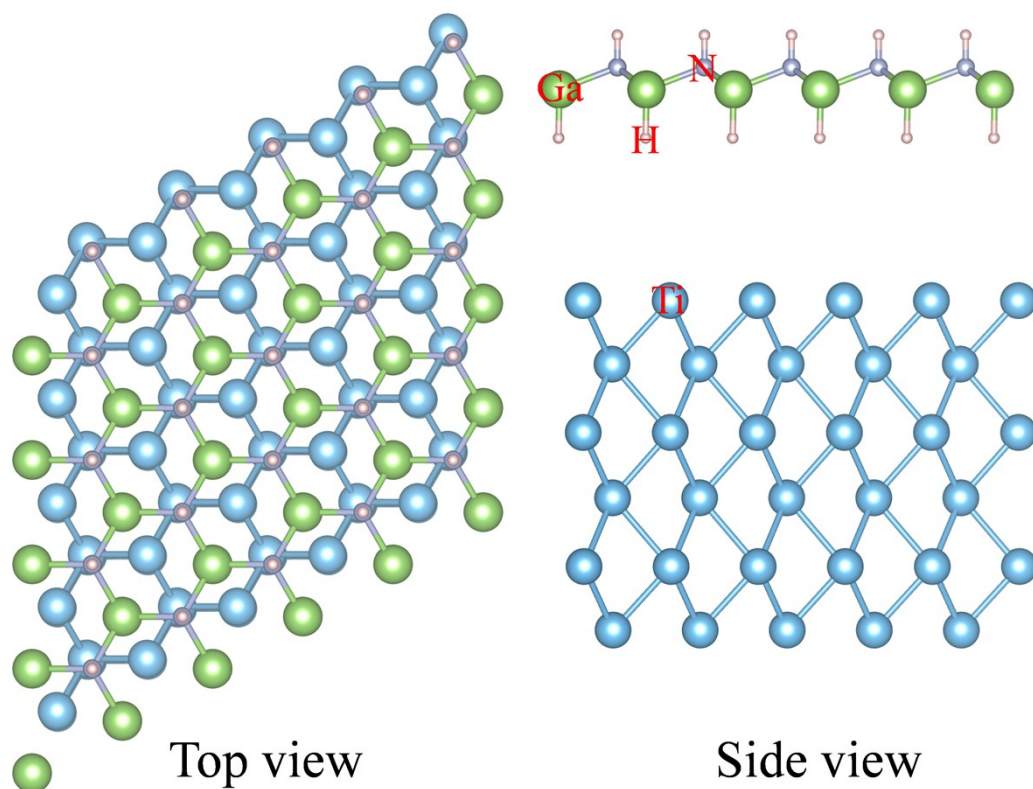
Figure S7. Atomic structures of HGaNH/Ti(0001) heterostructure.

It's well known that metal contacting, which is always needed when using 2d materials in real devices [30-36], is a crucial factor to affect the performance of 2d materials [30-36]. However, the formula to calculate μ_{2d} have some constraints [14, 24-25] and they are very difficult to extract reasonable data to quantitatively calculate the μ_{2d} of non-freestanding (means containing metal contacting) 2d materials. In addition, considering that there is no referable example for the metal contacting of pure (or fully-functionalization) monolayer GaN, we elaborately select the Ti(0001) electrode which is used to assemble nanodevices to qualitatively research this issue [29-35]. Based on this, a HGaNH/Ti(0001) heterostructure is built (Fig. S7). After geometry optimization (Fig. S7), there is no chemical bond between HGaNH and Ti(0001) electrode, indicating just a physical absorption. Thus, it is reasonable to assume that the C_{2d} of HGaNH does not significant change since HGaNH is physically absorbed on Ti(0001) surface (Fig. S7),

then the remaining key factors associated with μ_{2d} are E_1 an m^*. According to the formula of effective mass ($m^* = \hbar[\partial^2 E(k)/\partial^2 k]^{-1}$), m^* is directly related to the dispersion relation ($E(\boldsymbol{k})$-$\boldsymbol{k}$ cures) around CBM\VBM, so, to qualitatively inspect the change of $E(\boldsymbol{k})$-$\boldsymbol{k}$ cures, the decorated bandstructures of HGaNH/Ti(0001) heterostructure are shown in Fig. S8. Comparing Fig. S8a (the red lines) and Fig. 2b, the $E(\boldsymbol{k})$-$\boldsymbol{k}$ cures around VBM and quasi-VBM are similar, indicating the major hole m^* features of HGaNH should not bear dramatic change when the Ti(0001) electrode is added. In contrast to the similar VBM (or quasi-VBM) $E(\boldsymbol{k})$-$\boldsymbol{k}$ cures, the quasi-CBM $E(\boldsymbol{k})$-$\boldsymbol{k}$ cures of HGaNH in HGaNH\Ti(0001) are evidently different from that of free-standing HGaNH, implying the electron m^* of HGaNH in HGaNH\Ti(0001) have changed compared with that of pure HGaNH.

Furthermore, the wavefunction of quasi-CBM and quasi-VBM are calculated and plotted in Fig. S9. The wavefunction distribution (mainly stems from N-$p_x p_y$ orbitals) of quasi-VBM (Fig. S9b) resembles that of pure HGaNH (Fig. 4c), not only verifying the robust hole m^* (as mentioned above) but also demonstrating E_1 (also m^*) maintains its major features although HGaNH interacts with the Ti(0001) electrode. Similarly, although the CBM of HGaNH\Ti(0001) (Fig. S9a) maintain the characteristics of pure HGaNH (Fig. 3c) to some extent, the Ti atoms make a nonnegligible contribution to the quasi-CBM of HGaNH within HGaNH\Ti(0001), demonstrating E_1 (also m^*) ought to bear dramatic change when the Ti(0001) electrode is added. Thus, it is reasonable infer that the major hole μ features (isotropy or anisotropy) of HGaNH ought to be relatively robust about Ti electrode, while its electron μ features are susceptible to the Ti(0001) electrode.
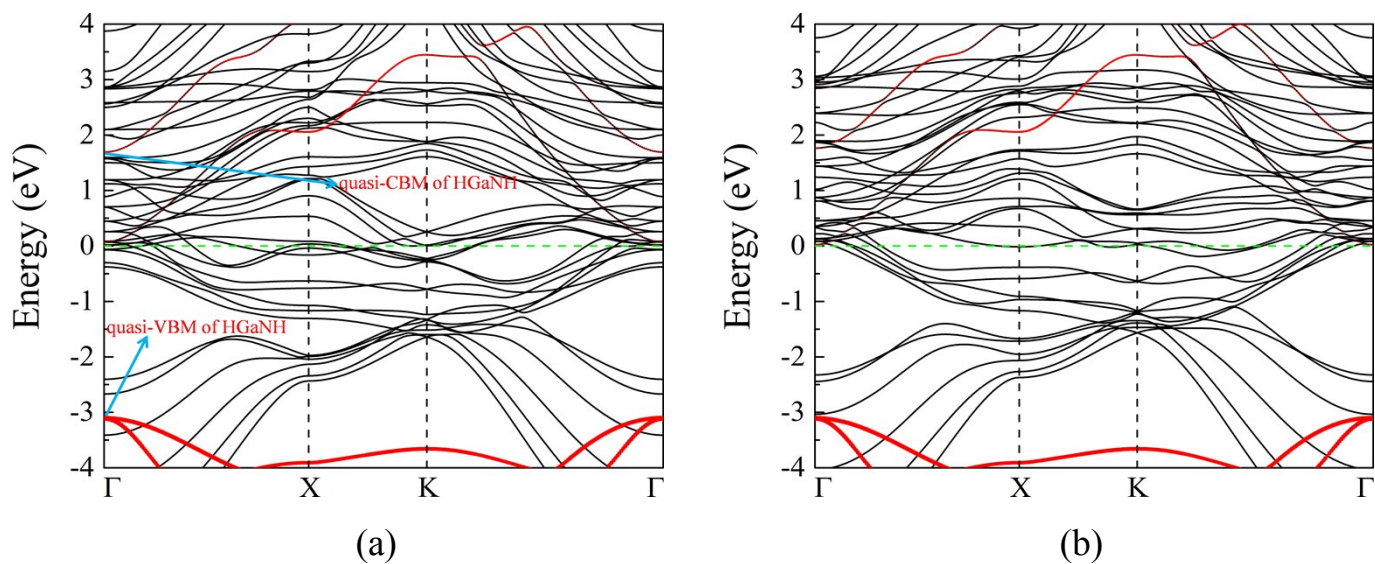
(a)　　　　　　　　　　　　　　　　(b)

Figure S8. Band structure of HGaNH/Ti(0001) heterostructure: (a) Spin up; (b) Spin down. The red color indicates the weight of a projection of the wave functions on the HGaNH sites.
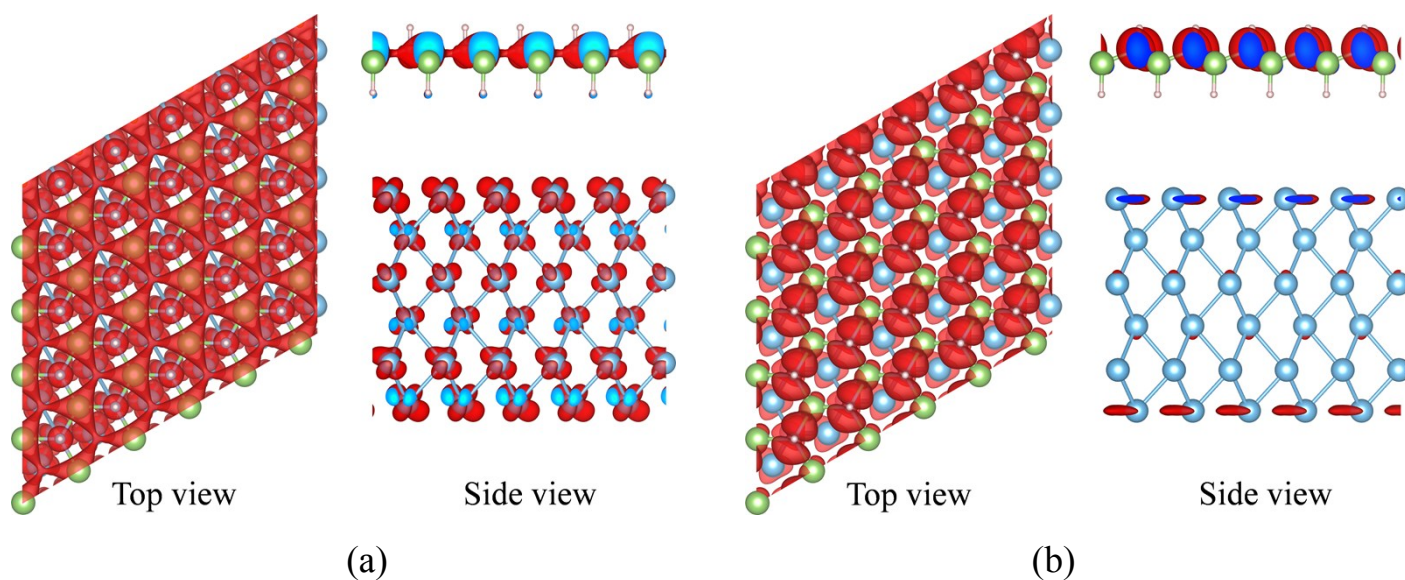

(a)　　　　　　　　　　　　　　　　(b)

Figure S9. The charge densities (top and side view) of HGaNH/Ti(0001) heterostructure. (a) for the quasi-CBM of HGaNH shown in Fig. S8a and (b) the quasi-VBM of HGaNH shown in Fig. S8a. The isosurface level is set at 0.02 e/Å^3.
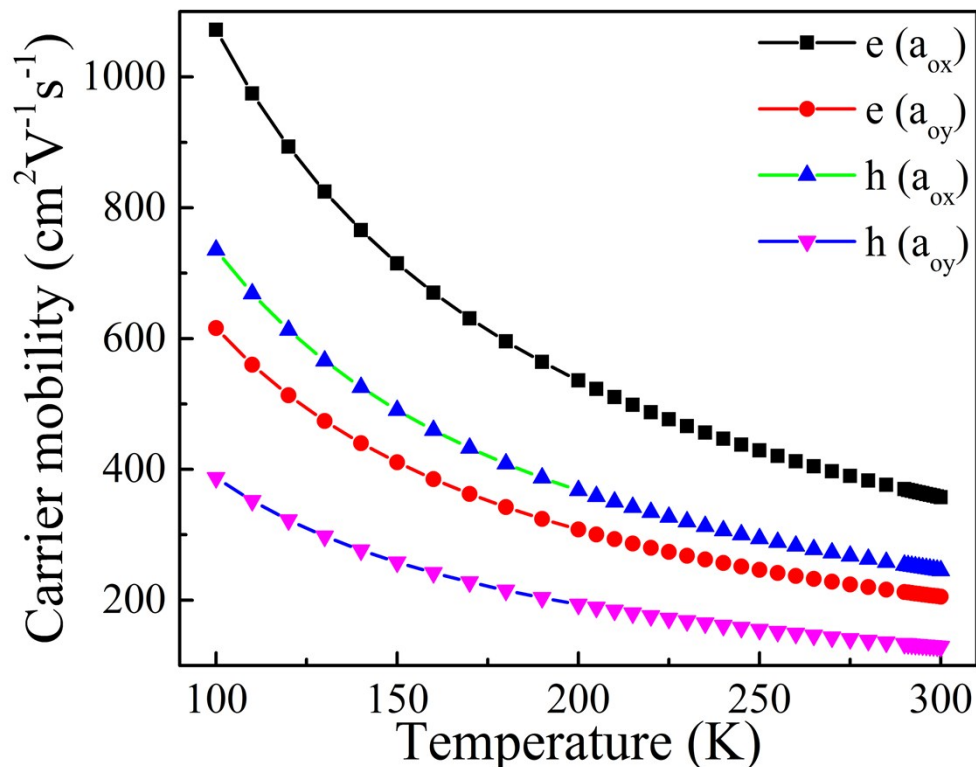
Figure S10. Temperature dependence of hole and electron mobilities along $\mathbf{a}_{ox}$ and $\mathbf{a}_{oy}$ directions for FGaNH.

References

[11] Qiao, J., et al., *High-mobility transport anisotropy and linear dichroism in few-layer black phosphorus*. Nat Commun, 2014. **5**: p. 4475.

[14] Cai, Y., G. Zhang, and Y.W. Zhang, *Polarity-reversed robust carrier mobility in monolayer MoS(2) nanoribbons*. J Am Chem Soc, 2014. **136**(17): p. 6269-75.

[16] Al Balushi, Z.Y., et al., *Two-dimensional gallium nitride realized via graphene encapsulation*. Nat Mater, 2016. 15(11): p. 1166-1171.

[24] Long, M.Q., et al., *Theoretical predictions of size-dependent carrier mobility and polarity in graphene*. J Am Chem Soc, 2009. **131**(49): p. 17728-9.

[25] Xi, J., et al., *First-principles prediction of charge mobility in carbon and organic nanomaterials.* Nanoscale, 2012. **4**(15): p. 4348-69.

[30] Giannazzo, F., et al., *Nanoscale current transport through Schottky contacts on wide bandgap semiconductors.* Journal of Vacuum Science & Technology B: Microelectronics and Nanometer Structures, 2009. **27**(2): p. 789.

[31] Giannazzo, F., et al., *Ambipolar MoS2 Transistors by Nanoscale Tailoring of Schottky Barrier Using Oxygen Plasma Functionalization.* ACS Appl Mater Interfaces, 2017. **9**(27): p. 23164-23174.

[32] Allain, A., et al., *Electrical contacts to two-dimensional semiconductors.* Nat Mater, 2015. **14**(12): p. 1195-205.

[33] Fontana, M., et al., *Electron-hole transport and photovoltaic effect in gated MoS2 Schottky junctions.* Sci Rep, 2013. **3**: p. 1634.

[34] Pan, Y., et al., *Monolayer Phosphorene–Metal Contacts.* Chemistry of Materials, 2016. **28**(7): p. 2100-2109.

[35] Su, J., et al., *The modulation of Schottky barriers of metal-MoS2 contacts via BN-MoS2 heterostructures.* Phys Chem Chem Phys, 2016. **18**(25): p. 16882-9.

[36] Zhong, H., et al., *Interfacial Properties of Monolayer and Bilayer MoS2 Contacts with Metals: Beyond the Energy Band Calculations.* Sci Rep, 2016. **6**: p. 21786.